CICE2023 Rio de Janeiro - Brazil 11TH INTERNATIONAL CONFERENCE ON FRP COMPOSITES IN CIVIL ENGINEERING

# SHEAR STRENGTH CONTRIBUTION PROVIDED BY INORGANIC-MATRIX COMPOSITES FULLY WRAPPED AROUND REINFORCED CONCRETE BEAMS

Veronica Bertolli, Politecnico di Milano, Italy, veronica.bertolli@polimi.it
Tommaso D'Antino, Politecnico di Milano, Italy, tommaso.dantino@polimi.it

## ABSTRACT
Fiber-reinforced cementitious matrix (FRCM) composites have been increasingly employed as externally bonded (EB) reinforcement for existing structures. FRCMs are effective in increasing the shear strength of existing concrete members. When the fully-wrapped configuration is employed, the composite tensile failure could be attained. In this paper, an analytical approach previously proposed to describe FRCM U-wrapped RC beams is extended to fully-wrapped members. This approach provides an accurate description of the stress-transfer mechanism between the FRCM bridging the shear crack and the substrate, thus allowing for an in-depth study of the composite contribution to the member shear strength.

## KEYWORDS
FRCM; shear strength; analytical model; stress transfer; bond

## INTRODUCTION
Fiber-reinforced cementitious matrix (FRCM) composites have gained large popularity in the past few years for strengthening concrete and masonry structures. They are applied as externally bonded reinforcement (EBR) and provide some advantages with respect to traditional retrofitting systems, such as high the strength-to-weight ratio, corrosion resistance, and ease of application (D'Ambrisi et al., 2013; Papanicolaou et al., 2008). They are comprised of high-strength fibers arranged in open-mesh textiles and embedded in an inorganic (lime-or cement-based) matrix, which is responsible of the good compatibility with concrete and masonry substrates. Different types of textile can be employed in FRCM, namely carbon, glass, basalt and polyparaphenylene benzobisoxazole (PBO) (Bencardino et al., 2018). The fibers provide the tensile strength, while the matrix is responsible for the stress-transfer between the textile and the matrix and between the FRCM and the substrate. The stress-transfer mechanism between the composite and substrate is usually described assuming a fracture mechanics pure Mode-II loading condition and debonding of the composite along one of the different interfaces involved (Carloni et al., 2018). The relationship between the relative displacement measured at the interface, i.e., the slip $s$, and the corresponding shear stress $\tau$, is referred to as the cohesive material law (CML). Once the CML is known, the bond behavior of a specific interface can be obtained. When one or two textile layers are employed, FRCM usually fails due to debonding of the textile from the embedding matrix, which prevents the full exploitation of the composite tensile strength. Indeed, the granularity of the inorganic matrix prevents complete impregnation of all fiber filaments within each bundle. The stress-transfer mechanism of the FRCM-substrate interface is a complex phenomenon affected by several parameters. For this reason, the FRCM bond behavior was extensively studied in the literature (Bertolli & D'Antino, 2022a; Focacci et al., 2017; Mirzaei et al., 2021; Misseri et al., 2021).

Externally bonded (EB) FRCM were proven to be an effective strengthening solution as they can improve bending (Brückner et al., 2006; Sneed et al., 2016), shear (Triantafillou & Papanicolaou, 2006), and torsional strength (Alabdulhady & Sneed, 2019) of existing reinforced concrete (RC) beams and provide confinement for columns (Ameli et al., 2022). Among the different applications, shear strengthening of existing concrete structures showed promising results in terms of increased shear strength and deformation capacity, shifting the typically quasi-brittle shear failure of RC beams to a pseudo-ductile shear failure, characterized by higher values of ultimate deflection with respect to

that of the unstrengthened element (Tetta et al., 2018). In the case of shear strengthening of RC beams with FRCM, the side-bonded, U-wrapped, or fully-wrapped configuration can be adopted. However, side-bonding is not recommended, as in (ACI Committee 549, 2020, p. 549) and (National Research Council, 2018), and full wrapping can be difficult if not impossible due to the presence of slabs. Therefore, U-jacket (where the composite is wrapped around three sides of the beam cross-section) is the most used configuration, although the contribution of FRCM composites may be limited by the occurrence of debonding. The fully-wrapped configuration provides the highest strength increase since composite tensile failure could be attained (D'Antino et al., 2022). Furthermore, it is particularly attractive in the case of RC columns, where the EB reinforcement can be easily applied. However, the contribution of fully-wrapped FRCM composites to the RC beam shear strength is still not clear and quite limited research on this topic can be found in the literature.

Following the approach adopted by design guidelines (ACI Committee 440, 2017; ACI Committee 549, 2020; National Research Council, 2017, 2018), the total shear strength of a RC beam with EB FRCM, $V_u$, is computed as:

$$V_u = V_c + V_s + V_f \quad \text{Eq. 1}$$

where $V_c$ and $V_s$ are the shear strength contributions provided by concrete and steel (if any), respectively, and $V_f$ is the composite shear strength contribution. (Eq. 1) assumes that the resisting mechanisms provided by concrete, steel, and composite attain their maximum value simultaneously and that the resisting mechanism of concrete and internal steel reinforcements remain the same with or without the EB reinforcement (Chen et al., 2013). These assumptions were proven to lead to non-conservative results for some FRP- and FRCM-strengthened beams (Gonzalez-Libreros et al., 2017; Pellegrino & Modena, 2002). Nevertheless, (Eq. 1) is commonly accepted in the literature (ACI Committee 549, 2020; National Research Council, 2018). The FRCM can be applied in a continuous or discontinuous layout, and the FRCM strips can have various widths and spacings. The textile is typically applied such that its longitudinal bundles are inclined at an angle ranging from 45° to 90° with respect to the longitudinal axis of the beam, and different number of FRCM layers can be employed. The shear strength contribution of the EB FRCM, $V_f$, is usually computed through the Mörsch truss model assuming that beam failure occurs with a main diagonal crack of inclination θ and that the FRCM jackets on opposite sides of the cross-section provide the same contribution (Figure 1).

$$V_f = 2nt_f\sigma_{fe}d_{fe}\frac{w_f}{i_f}(\cot\theta+\cot\beta)\sin\beta \quad \text{Eq. 2}$$

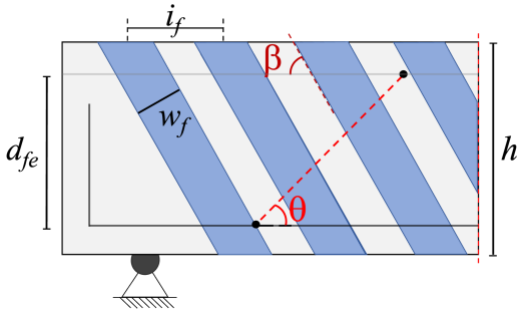


Figure 1: RC beam with fully-wrapped discontinuous FRCM

In (Eq. 2), $t_f$ is the equivalent thickness of the composite, $w_f$ the width of a strip (measured orthogonally to the), $i_f$ the strip spacing (measured orthogonally to the fiber longitudinal direction), $n$ is the number of textile layers, and β is the angle of the fibers with respect to the beam longitudinal axis. In the case of reinforcement continuous layout, $w_f=i_f\sin\beta$ holds. $d_{fe}$ is effective depth of the FRCM reinforcement and θ is the inclination of both the concrete strut and the main shear diagonal crack at failure (often assumed equal to 45° (D'Antino et al., 2020)). $\sigma_{fe}$ is the composite effective

stress, defined as the maximum average axial (i.e., fiber aligned) stress in the reinforcement bridging the shear crack.

In this paper, an analytical approach previously proposed to describe the actual stress distribution in a U-wrapped FRCM composite bridging the main shear crack of an RC beam (Bertolli & D'Antino, 2022b) is extended to the case of fully-wrapped FRCM. The approach analytically describes the stress-transfer mechanism between the composite and the substrate by assuming that the shear crack separates the FRCM strips in two joints, one above and one below the crack. Applying equilibrium and compatibility conditions to the different strips intersecting the crack, this approach provides the distribution of stress and slip along the crack, enabling a thorough description of the shear stress-transfer mechanism of the fully-wrapped EB FRCM. This will help in the assessment of formulas available in the literature to compute $V_f$.

## ROLE OF THE BOND BEHAVIOR IN THE DETERMINATION OF $\sigma_{fe}$

Following the definition of the composite effective stress, (Eq. 3) holds:

$$\sigma_{fe} = \frac{1}{\xi_1 - \xi_0} \max_{\alpha} \int_{\xi_0}^{\xi_1} \sigma(s, L) \mathrm{d}\xi \qquad \text{Eq. 3}$$

where $\xi$ is the coordinate along the main shear crack from the crack tip, $\xi$=0, to the crack end, $\xi=\xi_1$, while $\xi_0$ is the point where the composite intersects the crack closest to the crack tip ($\xi_0$=0 for the case of continuous layout). The maximum value of the integral in (Eq. 3) varies with the crack opening angle, $\alpha$. $\sigma(s, L)$ is the actual stress distribution in the composite bridging the shear crack and it is a function of the slip at crack, $s$, and of the bonded length available for each fiber from crack location. It should be noted that the composite configuration (side-bonded, U-wrapped, and fully-wrapped) affects the stress distribution $\sigma(s, L)$ and hence the value of $\sigma_{fe}$.

As usually assumed in the literature (Chen & Teng, 2003; D'Antino et al., 2020; Monti & Liotta, 2007), the critical shear crack is assumed to divide the composite in two different strips, one below and one above the crack. These can be regarded as two different FRCM-concrete joints connected at the shear crack, i.e., at their loaded end.

Both joints can be studied considering a fracture mechanics Mode-II loading condition. Their bond behavior is fully defined by their CML, geometry, and boundary conditions. The solution of the bond differential equations provides the slip, axial stress, and shear stress distributions along the joint interface. The debonding process of the joint can be described by axial stress $\sigma$ - global slip $g$ curves (also referred to as joint load responses), where $\sigma$ is the axial stress in the composite loaded end and $g$ is the composite-concrete relative displacement measured at the joint loaded end. In the description of the bond behavior, the constraints at the far end play a crucial role. When the composite strip is free at far end, the joint is defined as type A joint (Chen et al., 2012, 2017) and its idealized $\sigma_A$-$g_A$ curve is depicted in blue in Figure 2a. Conversely, when the composite strip is fixed at the far end the joint is defined as type B joint (Chen et al., 2012, 2017) and its idealized load response ($\sigma_B$-$g_B$ curve) is depicted in green in Figure 2a. Both curves have an initial elastic branch up to $\sigma_a$, followed by a softening branch ending when the bond stress-transfer mechanism is fully established ($\sigma_{deb}$). If friction at the debonding interface is present, as in the case of curves depicted in Figure 2a, the stress can further increase as the debonding crack propagates. Once the stress-transfer mechanism has reached the far end, the constraints of the specific type of joint starts to be effective. The axial stress of type A joint, after attaining the peak stress $\sigma^*$, starts to decrease as the stress debonding crack propagates. For type B joint, the fixed far end allows for further increasing the axial stress until the composite tensile strength $\sigma_{max}$ is attained. It is worth noting that the load responses reported in Figure 2 are referred to long bonded length joints (i.e., joint with bonded length $L$ greater that the effective bond length, $l_{eff}$). The detailed solution of the bond differential equation at each step of the debonding process and the

corresponding full-range analytical description of the σ - *g* curves can be found in the literature for different shape of the CML, e.g. (Bertolli & D'Antino, 2022a; Calabrese et al., 2019).

For each joint above (below) the critical shear crack, the distance between the crack axis ξ and the upper (lower) side of the composite measured in the direction of the longitudinal fibers is the bonded length, $L_a$ ($L_b$) (Figure 2b). The boundary conditions of joint above and below depend on the FRCM configuration adopted. When side bonding is adopted, both the joint above and below the crack are type A joints since they are simply bonded to the beam side. When U-wrapped configuration is employed, the joint above the crack is type A while that below is type B joint (D'Antino et al., 2020; Monti & Liotta, 2007), considering that the former is bonded to the beam while the latter wraps the beam bottom side. For the fully-wrapped configuration, both joints can be regarded as anchored to the beam, therefore only type B joints are considered (see Figure 2b).

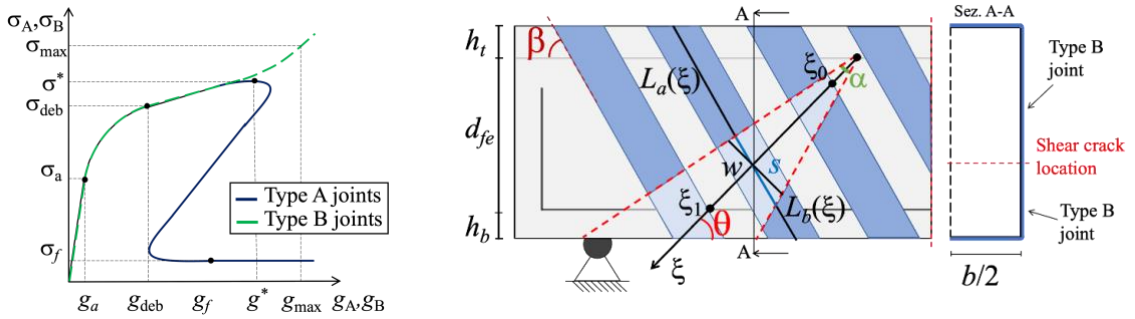


a) b)

Figure 2: a) Load responses of type A and B joints and b) crack opening for the case of fully-wrapped EBR

Some assumptions were made in the literature to analytically determine $\sigma_{fe}$. For U-wrapped FRCM, the strips above the crack were assumed to simultaneously reach their peak stress $\sigma^*$, while for fully-wrapped FRCM it was assumed that the tensile strength of the material was first attained at the mid-length of the crack. Nevertheless, interaction between the joint above and below the crack and the actual stress distribution in the fully-wrapped configurations need further investigations.

## ANALYTICAL APPROACH TO DETERMINE σ(ξ)

In this section, an analytical model to determine the actual stress distribution arising at the shear crack in the case of fully-wrapped composites is presented. The same approach was previously adopted for U-wrapped composites (Bertolli & D'Antino, 2022b). This model is based on (Eq. 2). Thus, it assumes: i) failure is attained due to the opening of a main diagonal crack, ii) the crack has a linear opening, which allows for computing the crack opening along the crack coordinate ξ as $w=\alpha\xi$ under the small displacement hypothesis, and iii) the crack tip is located at the centroid of the flexural compression zone and the crack end at the centroid of the longitudinal reinforcement. Along the crack coordinate ξ, each strip intersected by the crack is divided into two joints, one below and one above the crack. The crack opening *w* entails for the slip *s* at the FRCM-substrate interface along the crack, which is the sum of the slip of the joint above and of the joint below the crack. The slip in fiber direction was computed as $s=\alpha\xi\sin(\theta+\beta)$ (see Figure 2b). Joints above the crack have bonded length $L_a=\xi\sin\theta/\sin\beta+h_t/\sin\beta$, where $h_t$ is the distance between the extreme flexural compression fiber of the beam and the centroid of the flexural compression zone, while joints below the crack have bonded length equal to $L_b=(\xi_1-\xi)\sin\theta/\sin\beta+h_b/\sin\beta$, where $h_b$ is the distance between the extreme flexural tension fiber of the beam and the centroid of the longitudinal reinforcement (both measured in the direction orthogonal to the beam longitudinal axis, see Figure 2b). A suitable τ - s relationship (i.e., an interface CML) should be adopted to describe the joint bond behavior of the specific FRCM considered. For the case of full-wrapped configuration, only type B joints were considered (Chen et al., 2012). Although joints above and below the crack have the same boundary conditions at the far

end, they provide different load responses, i.e., different $\sigma_B$ - $g_B$ curves, due to the different bonded lengths of fibers at a specific $\xi$ coordinate.

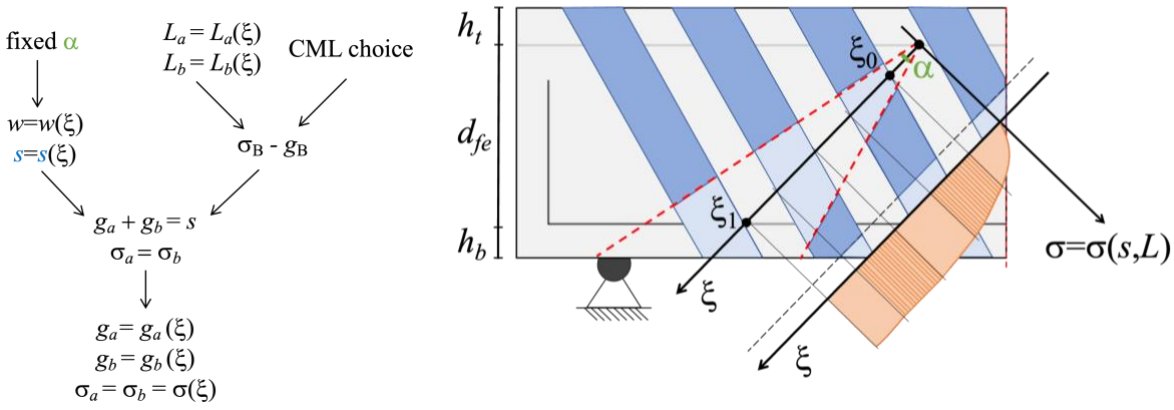


a) b)

Figure 3: Schematic description of the a) approach followed to determine the stress distribution along the crack for the case of fully-wrapped composites and b) its idealized representation

Provided $L_a$, $L_b$, and the interface CML, the load responses of joints above ($\sigma_a$ - $g_a$) and below ($\sigma_b$ - $g_b$) the crack can be obtained. The axial stress distribution along $\xi$ can be obtained enforcing compatibility and equilibrium conditions at the crack:

$$\begin{cases} g_a + g_b = s \\ \sigma_a = \sigma_b \end{cases} \qquad \text{Eq. 4}$$

Where $g_a$ and $g_b$ are the loaded end slips of the joint above and below the crack, respectively, and $\sigma_a$ and $\sigma_b$ are the corresponding stresses. The solution of the system of equation in (Eq. 5) provides the slip values at both side of the crack and the corresponding stresses in the composite. In this paper, (Eq. 5) was solved numerically for every fiber intersecting the crack from $\xi=\xi_0$ to $\xi=\xi_1$. Therefore, the slip distribution $g_a$ and $g_b$ as well as the composite axial stress distribution $\sigma=\sigma_a=\sigma_b$ along the crack coordinate $\xi$ were obtained. A schematic description of the approach followed is reported in Figure 3a. Increasing the value of the crack opening angle, the evolution of the stress-transfer mechanism between the composite and concrete across the crack could be obtained.

In this analytical model, the fibers that intersect the shear crack below the centroid of the longitudinal tension steel reinforcement (i.e., fibers located at $\xi>\xi_1$) were not considered in the shear strength provided by the composite, i.e., their corresponding stress $\sigma(\xi)$ was not considered to contribute to $\sigma(s,L)$. This assumption was adopted to provide a simple design equation for FRP and FRCM EB shear reinforcement (D'Antino et al., 2020; Monti & Liotta, 2007) and was considered in this paper to compare the results obtained with the model proposed with those of available design guidelines (National Research Council, 2018). However, strip portions associated with $\xi>\xi_1$ were accounted for when computing the bonded length of the different joints along the crack. The model proposed can be applied to any FRCM shear-strengthened beam (with different geometrical and mechanical properties), provided the full definition of the joint bond behavior (i.e., of its CML).

**RESULTS**

The analytical model described in the previous section was applied to a reference RC beam shear-strengthened with one layer of continuous PBO-FRCM using the fully-wrapped configuration. The beam had height $h$=500 mm and internal level arm $z$=0.9$d$=405 mm, $d$=450 mm being the cross-section effective depth. Considering the fully wrapped configuration, the effective depth of the FRCM shear reinforcement was $d_{fe}=z$=405 mm, where $d_{fe}$ is the depth associated with the total crack length $\Delta\xi$. Thus, considering the fully-wrapped configuration, $h_t$=45 mm and $h_b$=50 mm. The angle of the

compressed strut θ was assumed equal to 45° and the FRCM fibers were inclined with an angle β=70°. The PBO textile employed had cross-sectional area $A_f$=0.46 mm$^2$ and contact perimeter $p$=10 mm, while the elastic modulus and tensile strength were $E_f$=206 GPa and $\sigma_{max}$=3960 MPa (Bertolli & D'Antino, 2022a), respectively. The CML employed in the solution of the bond differential equation for the specific FRCM considered was a rigid-trilinear CML calibrated on the results of single-lap direct shear tests of PBO FRCM-concrete joints with three different bonded lengths (named CML2 in (Bertolli & D'Antino, 2022a)). The parameters that fully define the CML considered are reported in Table 1. It is worth noting that the CML employed entails for a finite value of the effective bond length and was proven to accurately fit the experimental results also in the case of FRCM-concrete joints with a fixed far end (Bertolli & D'Antino, 2022a).

Table 1: Rigid-trilinear CML employed

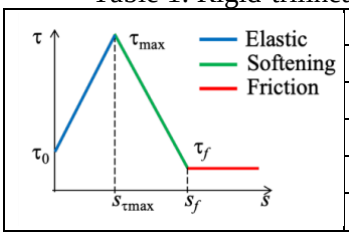


| CML parameters | |
|---|---|
| $\tau_0$ [MPa] | 0.04 |
| $\tau_{max}$ [MPa] | 0.74 |
| $\tau_f$ [MPa] | 0.04 |
| $s_{\tau max}$[mm] | 0.16 |
| $s_f$ [mm] | 1.14 |

The critical crack opening angle was defined as the value of α that maximizes the integral in (Eq. 3) and is associated with the composite shear strength maximum contribution, $V_f$. For the case of U-wrapped FRCM, the critical angle $\alpha_{cr,U}$ was defined as the value of the crack opening angle when the stress in the strip above the crack (type A joint) located at $\xi=\xi_1$ reaches its peak value, $\sigma^*$ (Bertolli & D'Antino, 2022b). The maximum stress value that can be attained in type B joints is the FRCM tensile strength $\sigma_{max}$, irrespectively of the joint bonded length. Therefore, for the case of fully-wrapped composites, the critical angle $\alpha_{cr,F}$ was defined as the crack opening angle associated with the attainment of $\sigma_{max}$ by a certain fiber along the crack. The value of $\alpha_{cr,U}$ and $\alpha_{cr,F}$ depends on several parameters, such as the beam height and effective depth, inclination of fibers β and crack θ, and bond behavior of the specific FRCM employed. Therefore, the location along the crack where $\sigma_{max}$ is first attained may vary (D'Antino et al., 2022). In this paper, $\alpha_{cr,F}$ was assumed as the crack opening angle associated with the attainment of $\sigma_{max}$ in the fiber above the crack located at $\xi=\xi_1$

**Slip distribution along ξ**

Figure 4 shows the slips $g_a$ and $g_b$ (and their sum, $s$) obtained solving (Eq. 5) along ξ for different values of the crack opening angle, namely $\alpha=\alpha_{cr,U}$, $\alpha=\alpha_{cr,F}$, and $\alpha>\alpha_{cr,F}$. Considering the load response of type B joints, an increase in the bonded length always determines an increase of the global slip for a given value of stress (Bertolli & D'Antino, 2022a). Thus, when $L_a<L_b$, the equilibrium condition is attained with $g_a<g_b$. Vice versa, when $L_a>L_b$ then $g_a>g_b$ When $L_a=L_b$, the load responses of joints above and below the crack are the same and the global slips of the joints are equal, i.e., $g_a=g_b=s/2$.

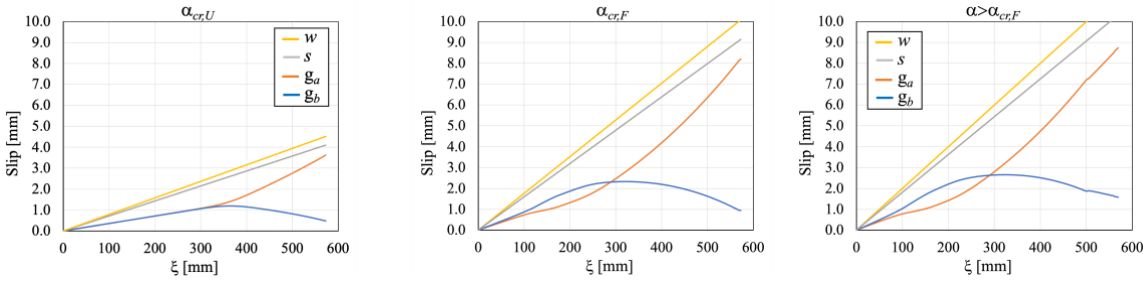


a) b) c)

Figure 4: Slip distribution along the crack for increasing values of α

**Shear stress distribution along ξ**

The shear stress τ along the crack in the two joints can be computed from the CML when the slips $g_a$ and $g_b$ are known. The τ distribution obtained along the crack for different values of α is reported in Figure 5. Figure 5 shows that, when $\alpha_{cr,F}$ was attained, debonding occurred in all fibers intersecting the crack for values of ξ greater than approximately 150 mm. Limited differences were observed for higher values of α.

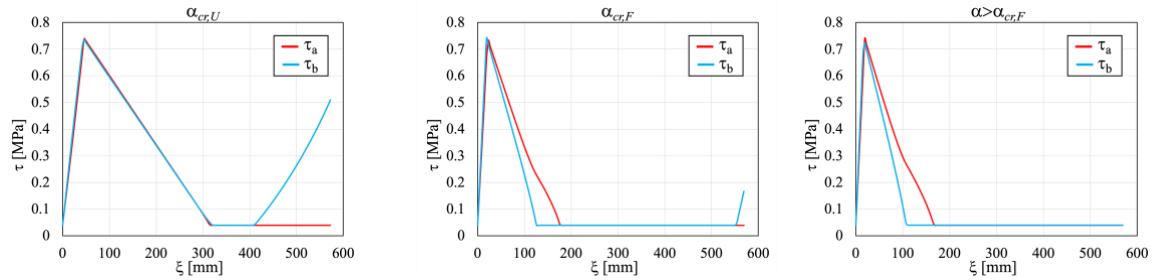


a) b) c)

Figure 5: Shear stress distribution along the crack for increasing value of α

**Axial stress distribution along ξ**

The axial stress distribution along the crack obtained by solving (Eq. 5) are reported in Figure 6. For the specific case considered, the tensile strength of the FRCM composite $\sigma_{max}$ was not attained in any fiber crossing the crack up to values of $\alpha=\alpha_{cr,U}$. When α reached $\alpha_{cr,F}$, the composite tensile strength was attained exactly at $\xi=\xi_1$. As α increased further, $\sigma_{max}$ was progressively attained by further fibers (Figure 6c).

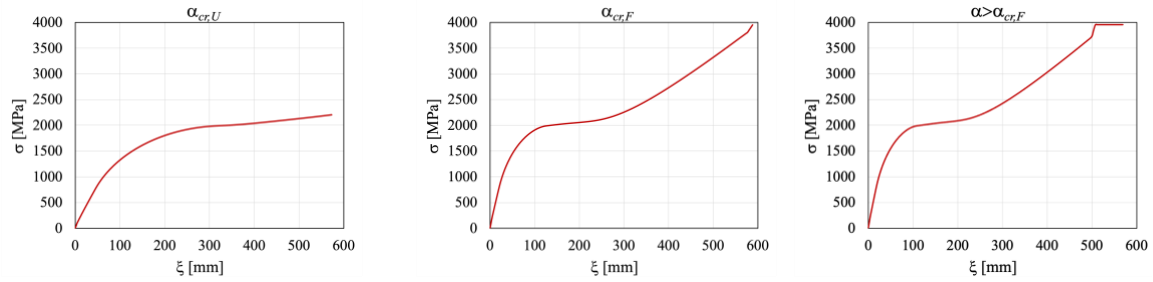


a) b) c)

Figure 6: Axial stress distribution along the crack for increasing value of α

**Evolution of the debonding process along fibers crossing the crack**

Starting from the slips $g_a$ and $g_b$ obtained for a given α, the evolution of the debonding process of every fibers along the crack could be obtained. Accordingly, the distribution of slip $s(x)$, axial stress $\sigma(x)$, and shear stress $\tau(x)$, along each fiber were determined for the reference beam considered .Figure 7 shows the portions of FRCM composite engaged in the elastic (blue), softening (green), and debonding (red) stage for increasing value of α. Figure 7 shows that, as α increases, the elastic, softening, and debonding stages advanced from the joint loaded toward the far end. It should be noted that the area engaged in the elastic stage could be identified due to the presence of the initial rigid branch of the CML employed.

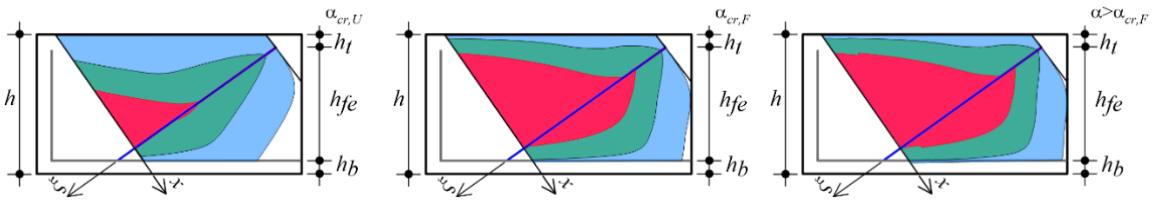


a) b) c)

Figure 7: Evolution of the debonding process in the composite intersecting the crack

## CONCLUSIONS

In this paper, an analytical approach was presented to compute the axial, i.e., fiber aligned, stress distribution in FRCM strips crossing the main shear crack of a fully-wrapped FRCM shear-strengthened RC beam. The axial stress distribution was obtained by equilibrium and compatibility conditions applied at the crack, based on the geometrical and mechanical properties of the strips. The model allowed to obtain slip, axial, and shear stress distributions in the composite along the crack, as well as a complete description of the debonding process of fibers intersecting the crack. The integral of the stress distribution along the crack, i.e., the effective stress $\sigma_{fe}$, could be employed to compute the shear strength contribution of the composite $V_f$ to the beam shear strength . The model proposed represents a valid tool to investigate the stress-transfer mechanism in the FRCM composite at crack when shear failure is attained. However, comparisons between values of crack opening associated with composite failure and those reached when concrete and steel attain their maximum contribution should be performed for different beam geometry and type of reinforcement. This will help studying the possible interaction between composite, concrete, and steel shear resisting mechanisms.

## CONFLICT OF INTEREST

The authors declare that they have no conflicts of interest associated with the work presented in this paper.

## DATA AVAILABILITY

Data on which this paper is based is available from the authors upon reasonable request.

## REFERENCES

ACI Committee 440. (2017). Guide to Design and Construction of Externally Bonded FRP Systems for Repair and Strengthening Concrete Structures. ACI 440.2R-17. ACI.

ACI Committee 549. (2020). Guide to Design and Construction of Externally Bonded Fabric-Reinforced Cementitious Matrix and Steel-Reinforced Grout Systems for Repair and Strengthening of Concrete Structures. ACI 549.4R-20. ACI.

Alabdulhady, M. Y., & Sneed, L. H. (2019). Torsional strengthening of reinforced concrete beams with externally bonded composites: A state of the art review. Construction and Building Materials, 205, 148–163. https://doi.org/10.1016/j.conbuildmat.2019.01.163

Ameli, Z., D'Antino, T., & Carloni, C. (2022). A new predictive model for FRCM-confined columns: A reflection on the composite behavior at peak stress. Construction and Building Materials, 337, 127534. https://doi.org/10.1016/j.conbuildmat.2022.127534

Bencardino, F., Carloni, C., Condello, A., Focacci, F., Napoli, A., & Realfonzo, R. (2018). Flexural behaviour of RC members strengthened with FRCM: State-of-the-art and predictive formulas. Composites Part B: Engineering, 148, 132–148. https://doi.org/10.1016/j.compositesb.2018.04.051

Bertolli, V., & D'Antino, T. (2022a). Modeling the behavior of externally bonded reinforcement using a rigid-trilinear cohesive material law. International Journal of Solids and Structures, 248, 111641. https://doi.org/10.1016/j.ijsolstr.2022.111641

Bertolli, V., & D'Antino, T. (2022b). Stress transferred at the main shear crack of reinforced concrete beams strengthened with U-wrapped inorganic-matrix composites. 549–556. Scopus.

Brückner, A., Ortlepp, R., & Curbach, M. (2006). Textile reinforced concrete for strengthening in bending and shear. Materials and Structures, 39(8), 741–748. https://doi.org/10.1617/s11527-005-9027-2

Calabrese, A. S., Colombi, P., & D'Antino, T. (2019). Analytical solution of the bond behavior of FRCM composites using a rigid-softening cohesive material law. Composites Part B: Engineering, 174, 107051. https://doi.org/10.1016/j.compositesb.2019.107051

Carloni, C., D'Antino, T., Sneed, L. H., & Pellegrino, C. (2018). Three-Dimensional Numerical Modeling of Single-Lap Direct Shear Tests of FRCM-Concrete Joints Using a Cohesive Damaged Contact Approach. Journal of Composites for Construction, 22(1), 04017048. https://doi.org/10.1061/(ASCE)CC.1943-5614.0000827

Chen, G. M., Li, S. W., Fernando, D., Liu, P. C., & Chen, J. F. (2017). Full-range FRP failure behaviour in RC beams shear-strengthened with FRP wraps. International Journal of Solids and Structures, 125, 1–21. https://doi.org/10.1016/j.ijsolstr.2017.07.019

Chen, G. M., Teng, J. G., & Chen, J. F. (2012). Process of debonding in RC beams shear-strengthened with FRP U-strips or side strips. International Journal of Solids and Structures, 49(10), 1266–1282. https://doi.org/10.1016/j.ijsolstr.2012.02.007

Chen, G., Teng, J.-G., & Chen, J.-F. (2013). Shear Strength Model for FRP-Strengthened RC Beams with Adverse FRP-Steel Interaction. Journal of Composites for Construction, 17(1), 50–66. https://doi.org/10.1061/(ASCE)CC.1943-5614.0000313

Chen, J.-F., & Teng, J.-G. (2003). Shear capacity of FRP-strengthened RC beams: FRP debonding. Construction and Building Materials, 17(1), 27–41. https://doi.org/10.1016/S0950-0618(02)00091-0

D'Ambrisi, A., Focacci, F., & Caporale, A. (2013). Strengthening of masonry-unreinforced concrete railway bridges with PBO-FRCM materials. Composite Structures, 102, 193–204. Scopus. https://doi.org/10.1016/j.compstruct.2013.03.002

D'Antino, T., Focacci, F., Sneed, L. H., & Pellegrino, C. (2020). Shear Strength Model for RC Beams with U-Wrapped FRCM Composites. Journal of Composites for Construction, 24(1), 04019057. https://doi.org/10.1061/(ASCE)CC.1943-5614.0000986

D'Antino, T., Sneed, L. H., & Focacci, F. (2022). Estimation of the Shear Strength of RC Members with Externally Bonded, Fully-Wrapped FRCM Composites. 10th International Conference on FRP Composites in Civil Engineering, 198, 597–608. https://doi.org/10.1007/978-3-030-88166-5_51

Focacci, F., D'Antino, T., Carloni, C., Sneed, L. H., & Pellegrino, C. (2017). An indirect method to calibrate the interfacial cohesive material law for FRCM-concrete joints. Materials and Design, 128, 206–217. Scopus. https://doi.org/10.1016/j.matdes.2017.04.038

Gonzalez-Libreros, J. H., Sneed, L. H., D'Antino, T., & Pellegrino, C. (2017). Behavior of RC beams strengthened in shear with FRP and FRCM composites. Engineering Structures, 150, 830–842. https://doi.org/10.1016/j.engstruct.2017.07.084

Mirzaei, A. M., Corrado, M., Sapora, A., & Cornetti, P. (2021). Analytical Modeling of Debonding Mechanism for Long and Short Bond Lengths in Direct Shear Tests Accounting for Residual Strength. Materials, 14(21), 6690. https://doi.org/10.3390/ma14216690

Misseri, G., Rovero, L., & Galassi, S. (2021). Analytical modelling bond behaviour of polybenzoxazole (PBO) and glass Fibre Reinforced Cementitious Matrix (FRCM) systems coupled with cement and gypsum matrixes: Effect of the Cohesive Material Law (CML) shape. Composites Part B: Engineering, 223, 109090. https://doi.org/10.1016/j.compositesb.2021.109090

Monti, G., & Liotta, M. (2007). Tests and design equations for FRP-strengthening in shear. Construction and Building Materials, 21(4), 799–809. https://doi.org/10.1016/j.conbuildmat.2006.06.023

National Research Council. (2017). Guide for the design and construction of externally bonded FRP systems for strengthening concrete structures. CNR DT 200/17. CNR.

National Research Council. (2018). Guide for the design and construction of externally bonded fibre reinforced inorganic matrix systems for strengthening existing structures. CNR DT 215/2018. CNR.

Papanicolaou, C. G., Triantafillou, T. C., Papathanasiou, M., & Karlos, K. (2008). Textile reinforced mortar (TRM) versus FRP as strengthening material of URM walls: Out-of-plane cyclic loading. Materials and Structures/Materiaux et Constructions, 41(1), 143–157. Scopus. https://doi.org/10.1617/s11527-007-9226-0

Pellegrino, C., & Modena, C. (2002). Fiber Reinforced Polymer Shear Strengthening of Reinforced Concrete Beams with Transverse Steel Reinforcement. Journal of Composites for Construction, 6(2), 104–111. https://doi.org/10.1061/(ASCE)1090-0268(2002)6:2(104)

Sneed, L. H., Verre, S., Carloni, C., & Ombres, L. (2016). Flexural behavior of RC beams strengthened with steel-FRCM composite. Engineering Structures, 127, 686–699. https://doi.org/10.1016/j.engstruct.2016.09.006

Tetta, Z. C., Triantafillou, T. C., & Bournas, D. A. (2018). On the design of shear-strengthened RC members through the use of textile reinforced mortar overlays. Composites Part B: Engineering, 147, 178–196. https://doi.org/10.1016/j.compositesb.2018.04.008

Triantafillou, T. C., & Papanicolaou, C. G. (2006). Shear strengthening of reinforced concrete members with textile reinforced mortar (TRM) jackets. Materials and Structures, 11.